

Excimer-laser-based lidar for tropospheric ozone monitoring

I. Veselovskii, B. Barchunov

Physics Instrumentation Center of General Physics Institute, Troitsk, Moscow Region, 142092, Russia
(E-mail: igorv@ns.pic.troitsk.ru)

Received: 26 June 1998/Revised version: 4 November 1998/Published online: 10 March 1999

Abstract. The description of ozone differential absorption lidar (DIAL) based on KrF and XeCl excimer lasers for day and night-time measurements in the troposphere is presented. The XeCl laser is used as the “off” wavelength emitter and the radiation of KrF laser is Raman-shifted in a hydrogen and deuterium cell to obtain 277 nm and 292 nm “on” wavelengths. For the measurements in the range 0.5–4.5 km the pair 277/308 nm is used and for 4–10 km range the pair 292/308 nm is applied. Simultaneously with the elastic backscattering, the Raman backscatter of the XeCl laser from nitrogen and water vapor are monitored. The nitrogen Raman signal is used for the calculation of aerosol backscattering and extinction coefficients and these are compared with the results derived from XeCl elastic backscatter by the Klett method. The aerosol profiles obtained are used for correction of ozone concentration. Some examples of lidar application for the investigation of diurnal and seasonal ozone variation are given.

PACS: 42.68.Rp; 93.85.+q; 94.10.Gb; 92.60.Jq

The importance of long-term measurements of tropospheric ozone is now well recognized and a network of ground-based monitoring stations is in operation throughout the world. Nevertheless for a fully representative picture of the tropospheric ozone, vertical sounding methods are necessary. Studies of photochemistry and ozone transport require regular diurnal measurements from the ground level up to tropopause with a height resolution of several hundred m and an accuracy of the order of 1 ppb. The capability of the DIAL technique for such monitoring was demonstrated about 15 years ago [1–3]. But in contrast to the stratosphere, where DIAL systems based on excimer lasers have become the routine instrument for stratospheric ozone monitoring [4–7] (see also references therein), the development of fully operational lidar systems and their application to the regular study of tropospheric ozone evolution were only started quite recently [8–13]. Such delay is related to the numerous problems to be solved before acceptable accuracy of the measurements had been achieved.

The main error source is high aerosol and trace gas concentrations in the troposphere and especially in the planetary boundary layer (PBL), so the choice of DIAL wavelengths for the sounding becomes very critical. If in stratospheric measurements the choice of XeCl laser as “on” wavelength source has no serious alternative today, in troposphere at least three types of laser sources have already proved their suitability for such measurements. These are tunable dye lasers [1, 3, 8, 9, 13, 15] and fixed-frequency UV lasers such as KrF excimer [2, 11, 14] or a frequency-quadrupled Nd:YAG [10, 12, 16] in combination with Raman shifting technique. Though tunable lasers allow one to choose the optimal wavelengths for the sounding, their energy-power capabilities are very limited. The sounding errors for KrF and frequency-quadrupled Nd:YAG lasers are similar, so the choice between these lasers is related mainly to the operation convenience inside the lidar station. The advantages of frequency-quadrupled Nd:YAG laser are general for solid-state systems: compactness, reliability, and long lifetime of all laser components. Otherwise the KrF laser possesses significantly higher output power and the numerous Stokes orders may be efficiently produced to choose the optimal DIAL wavelengths for every altitude range. Especial interest for application of excimer lasers is supported by recent progress in elaboration of new high-density ceramic laser tubes with long life of discharge and optical components [17], which meet the specification of lidar radiation sources. The excimer lasers are simpler in operation when compared with solid-state lasers: short-time operation of excimer lasers sufficient for tropospheric measurements may be produced without water cooling, the radiation parameters are stable with temperature variations, and the pauses between the soundings do not influence the output energy.

In this paper we present a description of an excimer laser based DIAL system designed in the Physics Instrumentation Center of General Physics Institute to provide ozone density distribution from near ground level up to the free troposphere. The lidar station is located in Troitsk, which is 20 km southwest from Moscow.

1 Description of the lidar

1.1 Radiation source

To optimize the measurement accuracy over different altitude ranges and ozone concentrations the wavelengths with different absorption cross sections are required. Aerosol loading is most prominent in the mixed layer, and a strong gradient in aerosol concentration often exists at the top of the mixed layer, so the backscatter error will be most significant there. The KrF excimer laser in combination with hydrogen and deuterium Raman shifters can efficiently generate the Stokes orders of 268, 277, 292, 313, and 319 nm. The detailed analysis of both statistical and systematic errors for the different combinations of these wavelengths is presented in [11, 18, 19]. For the measurements in PBL the pairs 268/292 nm (first two Stokes orders in deuterium) and 277/313 nm (first two Stokes orders in hydrogen) are usually chosen. These pairs possess high ozone differential absorption cross section and their choice is convenient from the practical point of view: each pair may be generated by a single Raman cell, which allows one to increase the radiated energy and simplifies the alignment procedure. The pair 268/292 nm provides smaller errors up to 2 km altitude, but because of the strong absorption at the 268 nm for the measurements above 2 km the pair 277/313 nm is preferable.

In our previous study [20] we compared the ozone profiles measured with 268/292 nm, 277/313 nm, and 277/292 nm wavelengths and found that under perfect weather conditions these pairs lead to similar results. For routine monitoring the traditional choice is 277/313 nm because the Raman conversion in hydrogen is more efficient and this pair allows us to produce measurements up to 5–6 km. In the new version of our lidar we included additional XeCl laser as an “off” wavelength source instead of 313 nm. The reasons for such a modification are:

- to increase the “off” beam energy to make day-time long-range measurements possible;
- to use nitrogen and water vapor Raman signals from the 308 nm wavelength to obtain additional information about the aerosol content for the correction of ozone profiles.

In the new modification of the lidar the pair 277/308 nm is used for the 0.5–4.5 km heights and the pair 292–308 nm for the 4–10 km range.

An assembly drawing of the lidar is shown in Fig. 1. The KrF and XeCl excimer lasers (PIC design) of 200 mJ and 80 mJ output energy respectively are operated at a 50 Hz repetition rate. The lasers fire simultaneously and the precision of temporal synchronization is better than 10 ns. The radiation of KrF laser is focused by lenses of 1 m focal length into hydrogen or deuterium Raman cells. The pressures in the hydrogen and deuterium cells are 1.5 atm and 40 atm, respectively, to optimize the conversion efficiency to 277 nm and 292 nm. The energy of KrF laser is insufficient to pump both cells simultaneously so the switching between the cell is produced by the totally reflecting mirror M which directs the beam into the deuterium cell when it is necessary. The Stokes orders are collimated by 2.5-m focal length spherical mirrors and directed vertically into the atmosphere through two steering mirrors which are mounted

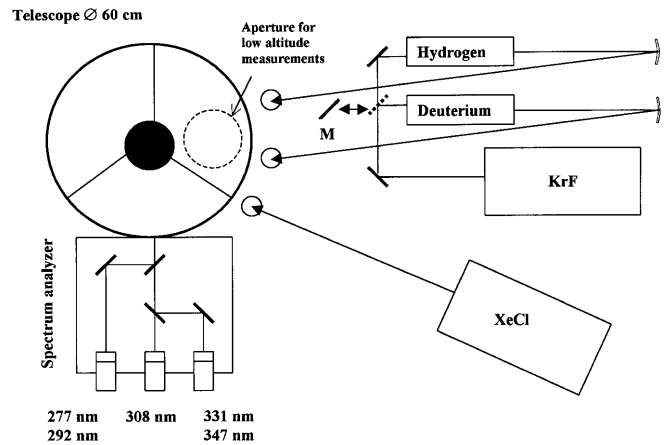


Fig. 1. An assembly drawing of lidar

to the side of the receiving telescope. The dielectric coatings of all turning mirrors are fully reflecting in the operational spectral range (268–319 nm) and transmitting the pump and high Stokes orders. The XeCl laser beam is twice expanded to keep the divergence smaller than 0.5 mrad. The divergence of 277-nm and 292-nm beams also did not exceed this value. The energy of laser pulses emitted in the atmosphere is 50 mJ at 277 nm, 30 mJ at 292 nm, and 70 mJ at 308 nm.

1.2 Receiving system

The radiation backscattered from the atmosphere is collected by a 60-cm-diameter Cassegrain telescope and enters into a spectrum analyzer. A lens with $f = 10$ cm is inserted after the field iris diaphragm to produce a collimated beam of 10 mm diameter. Dichroic mirrors divide the optical signal into three channels and the interference filters select the working wavelengths. The suppression of optical cross talks between the channels is better than 10^4 . The first channel is used for detection of 277-nm and 292-nm backscatter, the second for 308-nm backscatter, and the third for nitrogen and water vapor Raman signals (331 nm and 347 nm). Interference filters in the first and third channels can be easily replaced in accordance with the wavelengths used. The suppression of Rayleigh scattering in the Raman channel should be better than 10^7 , to achieve this value the additional absorption edge filter (hydroquinone dimethylether in ethanol) is used. The transmission bandwidth of the interference filters is about 3 nm except for 277 nm which is 5 nm. Despite the increased bandwidth the transmission at 277 nm is only 12%, which leads to a significant limitation in the maximum sounding altitude.

Optical signals are detected by PMTs operated in analog mode and digitized by a 12-bit 30-MHz ADC. To decrease the ADC's nonlinearities due to the differences in settling times of the internal comparators the dithering technique is applied in a way similar to that described in [21]. The ADC's modules are used with the standard VME bus and the controller accumulates a specified number of shots before the data are transferred to the main computer for storage and processing through the serial port.

1.3 Lidar operation

For the ozone density calculation we used the expression:

$$n_{oz} = -\frac{1}{2\Delta\sigma_{oz}} \frac{\partial}{\partial z} \ln \left[\frac{P_{on}(z)}{P_{off}(z)} \right] - \frac{1}{\Delta\sigma_{oz}} [\alpha_{on}^R - \alpha_{off}^R]. \quad (1)$$

Here $P(z)$ = light intensity returned from the range z ; $\Delta\sigma_{oz}$ = differential ozone absorption, $\alpha_{on,off}^R$ = Raleigh extinction coefficients for “on” and “off” wavelengths. Before the ozone calculation the integrated background is extracted from the backscattered signal separately for each channel. The background level is determined as a signal measured 20 μ s before laser firing. Raw lidar data are smoothed using Gaussian filters. The width of the filter window is usually kept to be 50 m. The derivative step Δz is changed with the altitude from $\Delta z = 50$ m for $z < 1$ km up to $\Delta z = 1$ km for $z > 8$ km.

One of the most serious source of errors in DIAL measurements is the signal-induced noise (SIN). The problem of SIN still has no satisfactory solution though different correction schemes were suggested [10, 13, 22]. The SIN originates from the intense PMT illumination from short-range scattered radiation. To prevent excessive anode current, the PMTs are electronically gated. The trigger pulse is applied to the dynodes near the photocathode 5 μ s before laser firing and the gain is lowered by a factor of 500. With the trigger pulse “off” the PMT reaches its normal gain during ≈ 600 ns. The operational current during the sounding never exceeded 1 mA. Nevertheless testing revealed that electronic gating had not removed the SIN problem completely, which led to the low values of ozone concentration at high altitudes. We found that this effect is decreased with the narrowing of the telescope field of view or at larger separation between the telescope and laser beams, which confirmed our suggestion about the excessive PMTs exposure. To overcome this problem, we used different fields of view for the telescope for high and low-altitude measurements.

The lidar signals could be processed only in the region of full overlap of area illuminated by lasers with the telescope field of view. The altitude H at which such overlap is achieved may be estimated as $H = 2D/(\varphi - \theta)$, where D is the maximum distance between the telescope and the laser beam edges, θ and φ are the beam divergence and telescope field of view. For the low-altitude measurements, we partly blocked the telescope with an aperture of 20 cm diameter close to the laser beams, as shown in Fig. 1. The field of view of the receiving telescope during low-altitude measurements is 1.5 mrad and full overlap is reached at altitudes smaller than 500 m. The voltage at the PMTs during these measurements is decreased. For the high-altitude measurements the full telescope aperture is used and the field of view is narrowed to 0.8 mrad. The example of adjusting of “low” and “high” altitude profiles for 277/308 nm pair is presented in Fig. 2. The delay between the measurements does not exceed 5 min. The precision of adjustment is good in spite of high and quickly changeable aerosol contents. The measurements with the apertured telescope are possible up to 2.5 km and with the open one up to 4.5 km. For the measurements above 4.5 km the pair 292/308 nm is used.

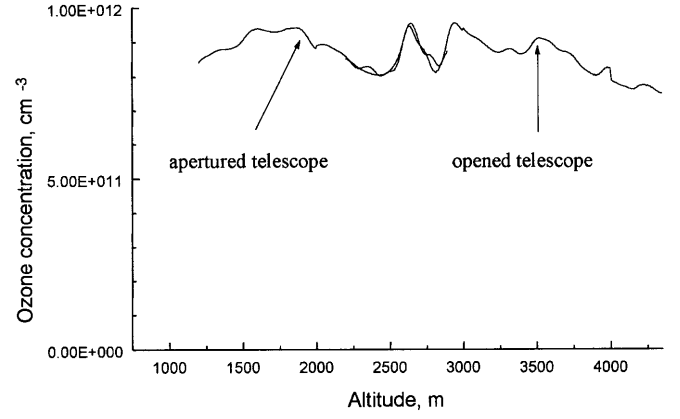


Fig. 2. Illustration of adjusting “low” and “high” altitude profiles for the 277/308 nm pair

2 Aerosol correction

Since high aerosol particles contents and high concentration gradients inside the boundary layer introduce significant error in the ozone measurements a correction for aerosol effects must be included. The correction terms to (1) may be calculated as [2]:

$$\Delta n_{oz} = \frac{1}{2\Delta\sigma_{oz}} \frac{\partial}{\partial z} \ln \left[\frac{\beta_{on}(z)}{\beta_{off}(z)} \right] - \frac{1}{\Delta\sigma_{oz}} [\alpha_{on}^A - \alpha_{off}^A], \quad (2)$$

with

$$\begin{aligned} \beta &= \beta^R + \beta^A \\ \beta_{on}^R &= \beta_{off}^R \left(\frac{\lambda_{off}}{\lambda_{on}} \right)^4 \\ \alpha_{on}^A &= \alpha_{off}^A \left(\frac{\lambda_{off}}{\lambda_{on}} \right)^k \\ \beta_{on}^A &= \beta_{off}^A \left(\frac{\lambda_{off}}{\lambda_{on}} \right)^\delta. \end{aligned}$$

Here, $\lambda_{off}, \lambda_{on}$ = unabsorbed and absorbed by ozone DIAL wavelengths, $\alpha_{on,off}^A$ = aerosol extinction coefficients for “on” and “off” wavelengths; $\beta_{on,off}^{A,R}$ = aerosol and Raleigh backscattering coefficients; k and δ are coefficients characterizing the wavelength dependence of aerosol parameters. The first term in (2) describes the differential backscattering error and the second one the aerosol differential extinction error. To evaluate the aerosol backscattering and extinction coefficients two independent methods of lidar equation inversion algorithms are applied: the Raman method [23–26] and the Klett method [27, 28].

2.1 Raman method

During the past decade the application of the Raman method for evaluation of aerosol parameters has been increasingly accepted. The main advantage of the Raman method is the possibility of simultaneous and independent measurement of the height profiles of the particle extinction and backscattering. Following Ansmann et al. [24] the aerosol extinction and

backscattering coefficients are calculated from the nitrogen Raman and elastic signals using the expression:

$$\alpha_{\lambda}^A(z) = \frac{\frac{\partial}{\partial z} \left\{ \ln \left[\frac{N_{N_2}(z)}{P_{N_2}(z)z^2} \right] \right\} - \alpha_{\lambda}^M(z) - \alpha_{N_2}^M(z)}{1 + \left(\frac{\lambda}{\lambda_{N_2}} \right)^k}, \quad (3)$$

$$\beta_{\lambda}^A(z) + \beta_{\lambda}^R(z) = \left[\beta_{\lambda}^A(z_0) + \beta_{\lambda}^R(z_0) \right] \times \left[\frac{P_{N_2}(z_0)P_{\lambda}(z)N_{N_2}(z)}{P_{N_2}(z)P_{\lambda}(z_0)N_{N_2}(z_0)} \right] \times \left\{ \frac{\exp \left[- \int_{z_0}^z \left(\alpha_{N_2}^A(\xi) + \alpha_{N_2}^M(\xi) \right) \partial \xi \right]}{\exp \left[- \int_{z_0}^z \left(\alpha_{\lambda}^A(\xi) + \alpha_{\lambda}^M(\xi) \right) \partial \xi \right]} \right\}, \quad (4)$$

where $P_{N_2}(z)$ is the intensity of nitrogen Raman scattering, λ, λ_{N_2} the wavelengths of elastic and nitrogen Raman scattering from nitrogen; $N_{N_2}(z)$ the nitrogen molecules number density; $\alpha_{\lambda, N_2}^{A, M}$ the aerosol and molecular extinction for elastic and Raman backscatters; ξ the variable of integration; z_0 is the reference altitude, where $\beta_{\lambda}^A(z_0) + \beta_{\lambda}^R(z_0) \approx \beta_{\lambda}^R(z_0)$. For UV wavelengths the Rayleigh scattering is the dominating process outside the boundary layer, so under good weather conditions we could choose the reference point below or above the cirrus cloud layer (7–11 km).

2.2 Klett method

The aerosol profiles are also derived from 308-nm backscatter by using the Klett numerically stable integration scheme [27, 28]. The aerosol backscattering coefficient can be calculated from the expressions:

$$\beta^A + \beta^R = \frac{\exp [S'(z) - S'(z_0)]}{\frac{1}{\beta^R(z_0)} + 2 \int_{z_0}^z R \{ \exp [S'(\xi) - S'(z_0)] \} \partial \xi},$$

$$S'(z) - S'(z_0) = S(z) - S(z_0) - \frac{16\pi}{3} \times \int_z^{z_0} \beta^R(\xi) \left(1 - R \frac{3}{8\pi} \right) \partial \xi - 2 \int_z^{z_0} \alpha^{oz}(\xi) \partial \xi, \quad (5)$$

where R is the aerosol lidar (extinction/backscattering) ratio and $S(z)$ is introduced as $S(z) = \ln [z^2(P(z))]$. To determine α and β values from the single equation the simple relationship between these coefficients is used:

$$\alpha(z) = R\beta(z).$$

More complicated relationships including range-dependent lidar ratio R are considered by many authors [28, 29] but at the present stage of software development we only use this simplest one. The integration is started at the upper end of the evaluation range and is carried out in 7.5-m steps. The contribution of ozone extinction for 308 nm in the boundary layer is not very critical and at this stage it was not considered. We

plan to do it in the future using an iteration scheme and the noncorrected ozone profile as initial one.

The relative behavior of the extinction profiles evaluated by the Raman and Klett methods are close, but the absolute value obtained from the Klett inversion is usually 15%–20% lower, which may be the result of numerous simplifications in our calculations. We believe that the Raman method leads to a more correct absolute value, since the only approximation in this method is the choice of the wavelength dependence of aerosol extinction. This discrepancy does not appreciably influence the results of ozone correction, but still we introduced an additional scale coefficient to adjust the profiles using the Raman one as a reference. Two extinction profiles obtained with Klett and Raman method in January 1998 are presented in Fig. 3. In this measurement 10^4 laser pulses are averaged, the derivative step is changed with the altitude from $\Delta z = 50$ m for $z < 1$ km up to $\Delta z = 1$ km for $z > 8$ km. The profile is typical for a winter: extinction inside the PBL is about 0.2 km^{-1} and the aerosol concentration distribution at the boundary layer top (≈ 2 km height) is quite smooth. Figure 4 presents the range dependence of lidar ratio R obtained the same day from the Raman measurements. Inside the boundary layer this value is about 25–30 and goes down with the altitude.

Raman method leads to more accurate absolute values of extinction and backscattering inside the boundary layer, but the error quickly increases with altitude because the Raman signal is three orders of magnitude weaker than the elastic one. To improve the accuracy, the number of accumulated laser pulses must be increased, which is unacceptable for the routine tropospheric monitoring. So we used Raman profiles only to check the absolute value of aerosol extinction in boundary layer and for the estimation of lidar ratio. For the correction of routine ozone measurements we used the Klett method with range-independent lidar ratio which is chosen to be 30 because the correction is most significant inside the PBL.

The application of aerosol correction to ozone profile measured on 18 November 1997 is illustrated by Fig. 5. For comparison, the same picture presents the corresponding profile of aerosol extinction evaluated by the Klett method. In this calculation the values $\delta = k = 1$ are used. The oscillations of ozone concentration in the 1–2.5 km altitude range originate mainly from aerosol differential backscattering and after

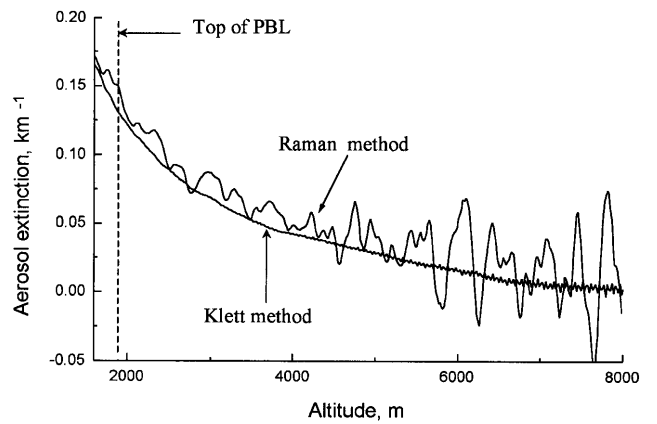


Fig. 3. Vertical profiles of aerosol extinction obtained with the Klett and Raman methods in January 1998

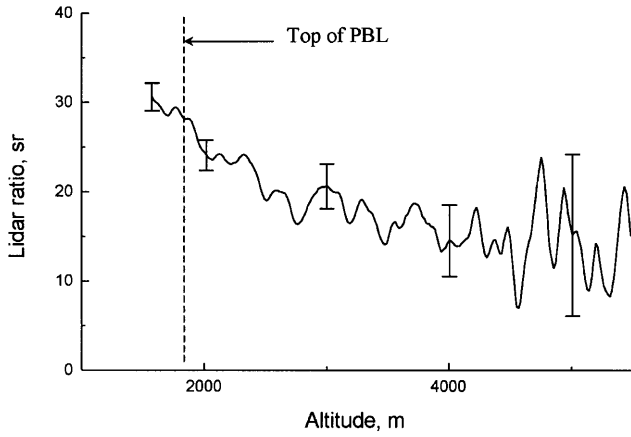


Fig. 4. Vertical profile of the extinction-to-backscatter ratio measured in January 1998

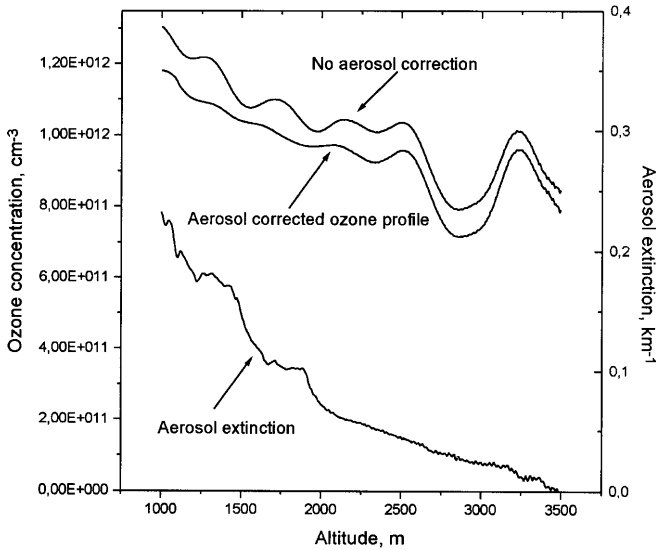


Fig. 5. Vertical ozone distribution obtained on 18 November 1997 with and without aerosol correction. For comparison, the corresponding profile of aerosol extinction is also presented

correction these are significantly decreased. The data processing without aerosol correction overestimates the ozone concentration inside PBL by $\approx 10^{-11} \text{ cm}^{-3}$. The correction of our data for differential backscattering is more or less successful for thin aerosol layers, but it basically does not work for the dense layers. During the ozone measurements we often observed the appearance of anomalies in ozone distribution such as peaks or dips, which were detectable during several hours. Aerosol correction is very important for distinguishing the real ozone effects from the artifacts caused by aerosol. For example in springtime an ozone dip at $\approx 1.5 \text{ km}$ altitude was frequently detected. But the origin of this dip is the high gradient of aerosol concentration at the top of the boundary layer and this dip is diminished after the aerosol correction.

2.3 Water vapor measurements

We also used the Raman channel for determination of the water vapor mixing ratio. The water vapor mixing ratio is

calculated as a ratio of water vapor and nitrogen Raman signals, corrected for aerosol and molecular differential absorption [24]:

$$n_{\text{H}_2\text{O}} = K \frac{P_{\text{H}_2\text{O}}(z)}{P_{\text{N}_2}(z)} \times \frac{\sigma_{\text{N}_2}}{\sigma_{\text{H}_2\text{O}}} \times \frac{\exp\left[-\int_{z_0}^z (\alpha_{\text{N}_2}^{\text{A}}(\xi) + \alpha_{\text{N}_2}^{\text{M}}(\xi)) \partial\xi\right]}{\exp\left[-\int_{z_0}^z (\alpha_{\text{H}_2\text{O}}^{\text{A}}(\xi) + \alpha_{\text{H}_2\text{O}}^{\text{M}}(\xi)) \partial\xi\right]}$$

where K is a system calibration constant, $\sigma_{\text{N}_2;\text{H}_2\text{O}}$ the Raman scattering cross sections; $\alpha_{\text{N}_2;\text{H}_2\text{O}}$ the extinction coefficients for the nitrogen and water vapor Raman signals. For the calculation of K we measured the transmittance of the water vapor and nitrogen Raman channels in a spectrum analyzer. Figure 6a shows the water vapor profile obtained in September 1997 with a height resolution of 50 m. When 10000 laser pulses are accumulated the measurements are possible up to 2–2.5 km altitude with the acceptable accuracy ($\pm 10\%$). For comparison Fig. 6b shows the aerosol extinction profile evaluated by the Klett method. It well illustrates that the structure of the extinction profile in this case is determined mainly by the water vapor contents. The regular water vapor measurements are the subject of future research for which the application of more powerful XeCl laser and comparison of results with sonde data are planned.

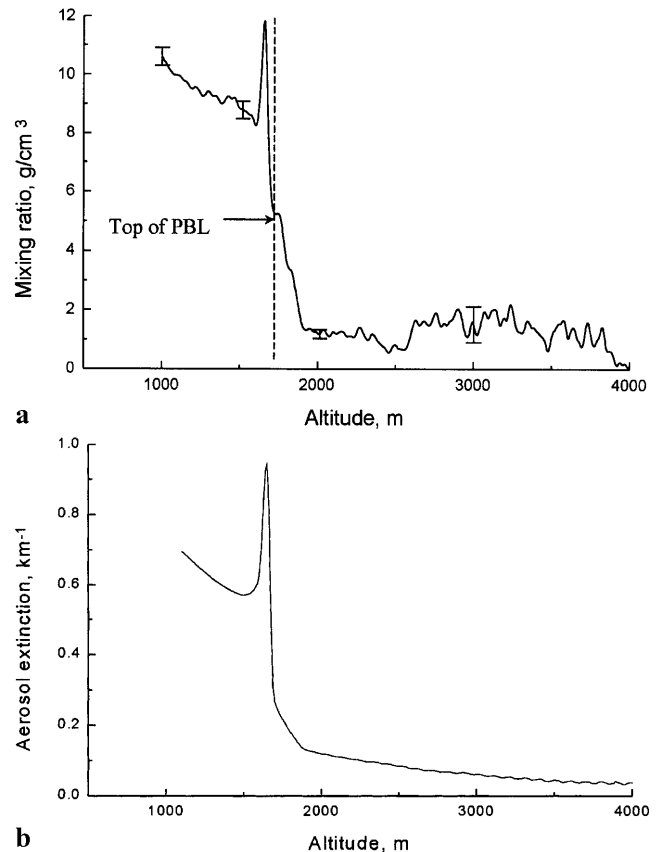


Fig. 6a,b. Water vapor profile measured by Rainan method (a) and extinction profile evaluated from elastic backscatter of XeCl laser by Klett method (b)

3 Routine ozone sounding

The testing of the modified lidar system was finished in June 1997 and since then regular measurements of ozone profiles were started. The main goal of these measurements is the investigation of seasonal and diurnal variations of ozone distribution in the troposphere. The measurements took place exclusively under fair-weather conditions.

The tropospheric ozone concentration in PBL depends on many factors, such as anthropogenic emissions, solar radiation, and atmospheric dispersion conditions. The averaged ozone concentration is higher in summer time and it is lower in winter. Usually ozone decreases with altitude and in the free troposphere the ozone densities were measured to be about half of the peak values in boundary layer.

Two typical ozone profiles obtained with the use of the 277/308 nm and 292/308 nm pairs are presented in Fig. 7. The delay between the measurements at these pairs does not exceed 15 min. For the 277/308 nm pair the number of accumulated pulses is 2000 and the maximal sounding altitude is 4.5 km. The 292/308 nm pair is applied for the 4–10 km range and, in a typical measurement, 10 000 pulses are averaged. Very often cirrus clouds limited the sounding range at 7–8 km. In the profile presented in Fig. 7b the peak in ozone concentration at 5.5 km and the dip at 6.5 km originate from the aerosol layer, which we were not able to correct completely.

The accuracy of the measurements in the lower troposphere (1–3 km) depends strongly on the aerosol loading and varies

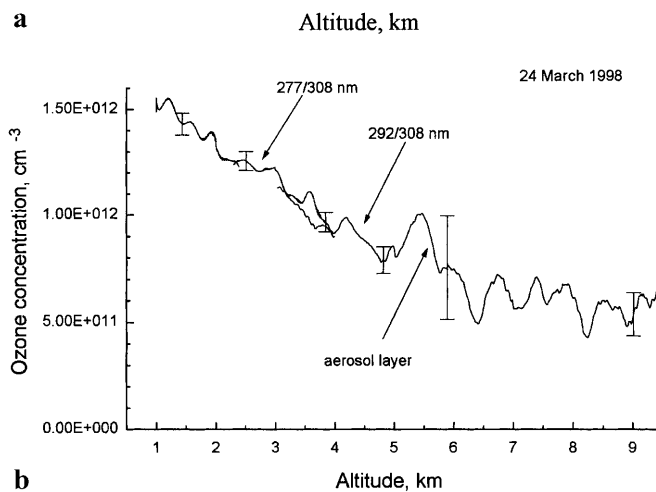
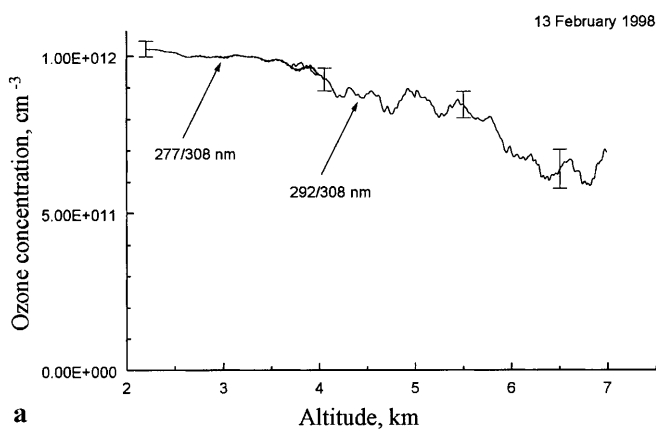


Fig. 7a,b. Ozone profiles measured on 13 February 1998 (a) and 24 March 1998 (b) with 277/308 nm and 292/308 nm pairs

from 5% in good visibility to 15% for haze. The error in the 3–6 km range is determined mainly by PMT nonlinearities and electronics noise and was about 15%. The increasing error up to 30% in the 6 km–10 km range is related to insufficient statistics. To improve the accuracy at high altitudes the energy of the 292-nm beam and the number of accumulated pulses must be increased. In our calculations we did not take into account the temperature dependence of the ozone absorption cross section and SO₂ gas differential absorption. The errors related to these factors are estimated to be smaller than 3%.

A strong diurnal cycle is generally found in polluted environments. It reflects the relationship between the buildup of ozone precursor gases in the early morning and the subsequent photochemical formation of ozone. In contrast to this, the clean environment usually exhibits a weak diurnal cycle. Also, ozone diurnal cycles in winter are usually weaker as compared with summer. We have already presented the results of our diurnal studies in [20]. In winter in stable weather conditions the diurnal ozone variations usually did not exceed 5%–10%. But when the weather is changing and especially when air masses arrive from Moscow these variations reached 20%–30%. So for the study of seasonal ozone variations we used daily averaged profiles. Figure 8 presents several ozone profiles measured on 20.02.1998 in the 12:00–19:30 time interval. The profiles are processed with a constant step $\Delta z = 100$ m.

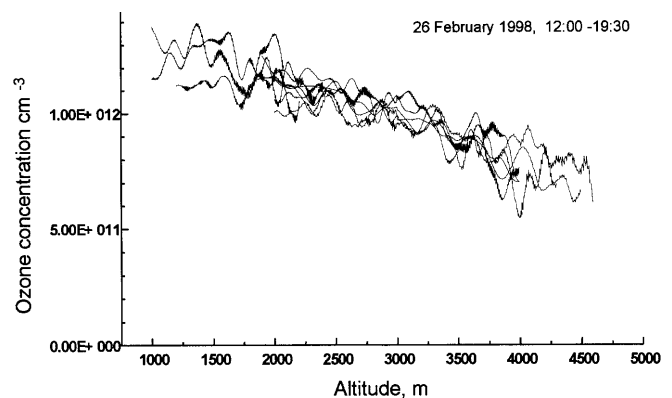


Fig. 8. Ozone profiles measured on 20 February 1998 in the 12:00 – 19:30 time interval. The profiles are processed with a constant step $\Delta z = 100$ m

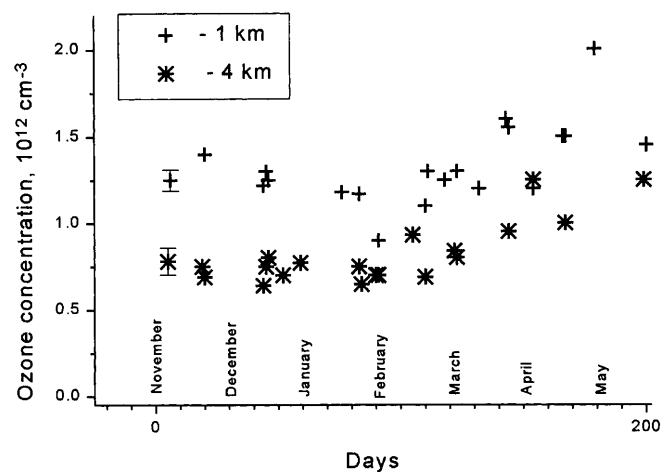


Fig. 9. Changes of ozone concentration at 1 km and 4 km altitudes during November 1997 – May 1998 period

summing we calculated the average values of ozone concentration in height intervals 500 ± 100 m, 1000 ± 200 m, 2000 ± 300 m, 3000 ± 400 m, and 4000 ± 500 m. Unfortunately we were unable to produce a whole day's measurements because of the weather conditions. Usually we sounded 5–6 times for a month during several hours so we could not completely exclude the influence of diurnal cycles on the results of day-to-day measurements. Figure 9 presents the seasonal changes of ozone concentration at 1 km and 4 km altitudes during the November 1997 – June 1998 period. The ozone concentration is minimal in winter and by summer it is increased almost twice.

4 Conclusion

The results, obtained during almost one year of operation of our modified lidar system, demonstrate that the use of additional XeCl laser makes it possible to increase the maximum range of the measurements up to 10 km. The Raman channel allows us to evaluate the water vapor contents in the boundary layer and the aerosol extinction and backscattering profiles. Application of aerosol correction decreases the measurement error in PBL but the corresponding program demands further improvements: the range-dependent lidar ratio and the ozone absorption must be included in the Klett method; more complicated dependences of aerosol parameters on the wavelength must be also considered. At present we continue the upgrading of the system simultaneously with the regular ozone measurements. In the near future the comparison of lidar profiles with the ozone sonde data is planned.

References

1. J. Pelon, G. Megie: *J. Geophys. Res.* **87**, 4947 (1982)
2. O. Uchino, M. Tokunaga, M. Maeda, Y. Miyazoe: *Opt. Lett.* **8**, 347 (1983)
3. E.V. Browell, A.F. Carter, S.T. Shipley, R.J. Allen, C.F. Butler, M.N. Mayo, J.H. Siviter, Jr., W.M. Hall: *Appl. Opt.* **22**, 522 (1983)
4. I.S. McDermid, T.D. Walsh, A. Deslis, M.L. White: *Appl. Opt.* **34**, 6201 (1995)
5. W. Steinbrecht, A.I. Carswell: *J. Geophys. Res. D* **100**, 1215 (1995)
6. L. Stefanutti, F. Castagnoli, M. Del Guasta, M. Morandi, V.M. Sacco, L. Zuccagnoli, S. Godin, G. Megie, J. Porteneuve: *Appl. Phys. B* **55**, 3 (1992)
7. T.J. McGee, M. Gross, U.N. Singh, J.J. Butler: *Opt. Eng.* **34**, 1421 (1995)
8. E.V. Browell, G.L. Gregory, R.C. Harris, V.W.J.H. Kirchhoff: *J. Geophys. Res. D* **95**, 16887 (1990)
9. E.V. Browell, M.A. Fenn, C.F. Butler, W.B. Grant, R.C. Harris, M.C. Shipham: *J. Geophys. Res.* **99 D**, 1739 (1994)
10. J.A. Sunesson, A. Apituley, D.P.J. Swart: *Appl. Opt.* **33**, 7045 (1994)
11. U. Kempfer, W. Carnuth, R. Lotz, T. Tricl: *Rev. Sci. Instrum.* **65**, 3145 (1994)
12. M. Beekmann, G. Ancellet, D. Martin, C. Abonnel, G. Duverneuil, F. Eideliman P. Bessemoulin, N. Fritz, E. Gizard: *Atmos. Env.* **29**, 1027 (1995)
13. M.H. Proffitt, A.O. Langford: *Appl. Opt.* **36**, 2568 (1997)
14. E. Wallinder, H. Ender, P. Ragnarson, S. Svanberg: *Phys. Scr.* **55**, 714 (1997)
15. Uta-B. Goers: *Opt. Eng.* **34**, 3097 (1995)
16. I.S. McDermid, D.A. Haner, M.M. Kleiman, T.D. Walsh, M.L. White: *Opt. Eng.* **30**, 22 (1991)
17. H. Ender, R. Patzel, U. Rebhan, M. Powell, D. Basting: *Jpn. J. Appl. Phys.* **34**, Part 1, 4050 (1995)
18. T. Shibata, T. Fukuda, T. Narikiyo, M. Maeda: *Appl. Opt.* **26**, 2604 (1987)
19. A. Papayannis, G. Ancellet, J. Pelon, G. Megie: *Appl. Opt.* **29**, 467 (1990)
20. I.A. Veselovskii, V.S. Bukreev, S.K. Vartapetov, Y.S. Shablin, H. Cha, D. Kim, K. Song, J. Lee: *J. Korean Phys. Soc.* **30**, 563 (1997)
21. A.O. Langford: *Appl. Opt.* **34**, 8330 (1995)
22. L. Fiorani, B. Calpini, L. Jaquet, H. Van den Bergh, E. Durieux: *Appl. Opt.* **36**, 6857 (1997)
23. U. Wandinger, A. Ansmann, J. Reichhardt, T. Deshler: *Appl. Opt.* **34**, 8315 (1995)
24. A. Ansmann, M. Riebesell, U. Wandinger, C. Weitkamp, E. Voss, W. Lahmann, W. Michaelis: *Appl. Phys. B* **55**, 18 (1992)
25. M.R. Gross, T.J. McGee, U.N. Singh, P. Kimvilakani: *Appl. Opt.* **34**, 6915 (1995)
26. T. Shibata, T. Sakai, M. Hayashi, T. Ojio, Soung-An Kwon, Y. Iwasaka: *J. Geomag. Geoelectr.* **48**, 1137 (1996)
27. J.D. Klett: *Appl. Opt.* **20**, 211 (1981)
28. J.D. Klett: *Appl. Opt.* **24**, 1638 (1985)
29. V.A. Kovaliov: *Appl. Opt.* **32**, 6053 (1993)